Egyptian Journal of Geology, v. 63, 2019, p.191-213

PETROLOGY AND GEOCHEMISTRY OF UM ESH OPHIOLITE SERPENTINITES, EASTERN DESERT, EGYPT: A NEOPROTEROZOIC METAMORPHOSED SSZ MANTLE

Ayman E Maurice

Geology Department, Faculty of Science, Helwan University, 1795 Cairo, Egypt

ABSTRACT

The Um Esh Neoproterozoic ophiolite serpentinites, Eastern Desert of Egypt, comprise massive and foliated varieties which are composed mainly of antigorite with accessory Cr-spinel. Carbonates are variable in abundance and represented by magnesite aggregates and veinlets. The Cr-spinels are usually zoned with fresh cores or relics surrounded by ferritchromite and chromian magnetite rims. The very low TiO_2 contents (<0.025 wt%) of primary Cr-spinel and the low Al_2O_3/SiO_2 values (0.010-0.016) of serpentinite samples are consistent with residual mantle which experienced high degree of partial melting. The Al_2O_3 (16-25 wt%) and TiO_2 (average = 0.007 wt%) contents of the primary Cr-spinel overlap those of spinels of suprasubduction zone (SSZ) and mid-oceanic ridge (MOR) peridotites. However, the Cr# (0.55-0.66) and Mg# (0.39-0.59) of the fresh Cr-spinels together with depleted nature of the Um Esh serpentinites are similar to those of modern SSZ fore-arc peridotites. Profiles along zoned Cr-spinels revealed that Cr_2O_3, Al_2O_3 and MgO abundances decreased abruptly, whereas FeO contents and Fe# ($Fe^{3+}/Cr+Al+Fe^{3+}$) increased rapidly from fresh Cr-spinel through ferritchromite to chromian magnetite, with gradual change within the individual metamorphic spinel zones. On the other hand, the variation of MnO and NiO abundances is not regular from core to rim. The dominance of antigorite and the presence of metamorphic spinel rims suggest that Um Esh serpentinites have experienced prograde metamorphism up to lower amphibolite facies under oxidizing conditions.

Keywords: Neoproterozoic mantle, SSZ ophiolites, serpentinites, Cr-spinel, Eastern Desert.

INTRODUCTION

Ophiolites are remnants of ancient oceanic lithosphere (upper mantle and crust) obducted into the continental margins. Typical ophiolite sections include residual mantle peridotites and magmatic rocks, which are topped by deep sea sediments known as pelagic sediments. The magmatic rocks comprise layered and isotropic gabbros followed by sheeted dykes and massive and pillowed basalts. According to their tectonic settings, ophiolites are classified into subduction-unrelated and subduction-related types (Dilek and Furnes, 2011, 2014; Pearce, 2014), which differ in the nature of their mantle sections and the composition of their magmatic rocks (Dilek and Furnes, 2014; Pearce, 2014).

The ophiolites of the Arabian-Nubian Shield, including the Egyptian ones, represent remnants of Neoproterozoic oceanic lithosphere, which were tectonically emplaced during closing of Mozambique Ocean existed between East and West Gondwana (Stern, 1994). The ophiolites of Egypt are present in the southern and central segments of the Eastern Desert. On the other hand, the existence of ophiolitic rocks in the North Eastern Desert and Sinai is controversial (Shimron, 1981, 1984; Abdel Khalek et al., 1994; Madbouly, 2000; Takla et al., 2001; Abu El-Enen and Makroum 2003; El Amawy et al., 2004; Mehanna et al., 2004). The ophiolites of Eastern Desert are mostly present as dismembered units, however, complete ophiolite sections were described from Fawakhir in the Central Eastern Desert (e.g. El-Sayed et al., 1999) and Wadi Ghadir in the South Eastern Desert (e.g. El-Sharkawy and El-Bayoumi, 1979). They comprise extensively serpentinized mantle peridotites, Moho transition zone rocks, metagabbros and massive and pillowed metabasalts (e.g. Zimmer et al., 1995; Azer and Stern, 2007; Basta et al., 2011; Gahlan et al., 2012; Ahmed, 2013; Khedr and Arai, 2017). Sheeted dykes and pelagic sediments are occasionally described from some ophiolites (e.g. Fawakhir, Wadi Ghadir and Gerf ophiolites, El-Sharkawy and El-Bayoumi, 1979; Basta et al., 2011; Abd El-Rahman et al., 2009; Zimmer et al., 1995).

Dating of Eastern Desert ophiolites indicates Neoproterozoic age (~730 to ~ 750 Ma). U-Pb zircon dating of the ophiolites of the Central (Fawakhir) and South (Wadi Gadir, Gerf and Allaqi) Eastern Desert produced similar ages. TIMS U-Pb zircon dating of Fawakhir ophiolitic gabbro gave 736.5 ± 1.5 Ma (Andresen et al., 2009). Similarly, Allaqi ophiolites were dated at 730 ± 6 Ma (Ali et al., 2010) using SHRIMP U-Pb zircon dating of layered ophiolitic gabbro. Kröner et al. (1992) used single grain zircon evaporation technique to date Wadi Ghadir and Gerf ophiolites at 746 ± 19 Ma and 741 ± 21 Ma, respectively.

Subduction-related and subduction-unrelated settings were proposed for the origin of the Egyptian ophiolites. Generally, these ophiolites are classified as supra-subduction zone types (e.g. Basta et al., 2011; Khedr and Arai, 2017), however, fore-arc (e.g. Azer and Stern, 2007; Abdel-Karim et al., 2016) and back-arc (e.g. Abd El-Rahman et al., 2009; Basta et al., 2011) settings are debated. On the other hand, some Egyptian ophiolites (e.g. Gerf, Zimmer et al., 1995) were considered to belong to Mid-Ocean Ridge (MOR) subduction-unrelated type. Moreover, different settings were proposed for the different rocks of Gerf ophiolite; fore-arc for ultramafic rocks (Abdel-Karim et al., 2016), back-arc for gabbros and major ocean basin for the sheeted dykes and pillow lavas (Zimmer et al., 1995).

This contribution presents mineral chemistry of primary and secondary minerals, and whole rock geochemistry of ophiolitic ultramafic rocks of Um Esh area, Central Eastern Desert, Egypt, aiming to evaluate the nature of a Neoproterozoic mantle and infer the tectonic setting of such ophiolitic rocks. Metamorphism of serpentinites and element mobility during Cr-spinel alteration has been evaluated.

GEOLOGIC SETTING

Wadi Um Esh area (Fig. 1) is a part of the Wadi Atalla district, which is characterized by NW-trending Atalla shear zone. Wadi Atalla and the surrounding areas represent a western end of the Precambrian rocks of the Central Eastern Desert of Egypt and have been the focus of several geological, geochemical, geochronological and isotopic studies, especially those concerned with the origin of gold mineralization in old gold mines such as Atalla, El-Sid and Fawakhir (e.g. Bakhit, 1994, 2001; Harraz, 1995; Taman, 1996; Zoheir et al., 2018), and fluorite mineralization as in Wadi Um Esh El-Zarga area (Taman, 1996). The Wadi Um Esh area is covered by several units of the Precambrian basement complex of Egypt, which include gneisses and migmatites, serpentinites and related rocks, metagabbro-diorite complex, mafic metavolcanics, metasediments (metamudstones), Hammamat molasse sedimentary rocks and younger granites (Wassef et al., 1973; Taman, 1996). Vein-type fluorite mineralization follows fault zone within the metagabbro-diorite mass (Wassef et al., 1973).

The ophiolitic ultramafic rocks (serpentinites and alteration products) constitute NW-trending belt parallel to Atalla shear zone, extending from Fawakhir granitic pluton in the southeast to Atalla gold mine in the northwest. These ultramafic rocks have structural contacts against the metagabbro-diorite complex, mafic metavolcanics and metasdiments (metamudstones) and are intruded by the younger granites. Akaad and Noweir (1980) proposed that the metagabbro-diorite complex is equivalent to the El Sid ophiolitic metagabbro of the Fawakhir ophiolite. The ophiolitic ultramafic rocks consist of serpentinites and talc-carbonates. The serpentinites are fine-grained and comprise massive and foliated varieties. They vary in colour from dark grey to greenish grey or reddish brown and are variably altered to brown foliated talc carbonate rocks, which occasionally have cavernous appearance.

PETROGRAPHY

The ultramafic rocks of Um Esh are classified into massive and foliated serpentinites and talc-carbonates. The serpentinites are fine-grained, composed of interlocking antigorites (Fig. 2A) with accessory Cr-spinel. In the foliated serpentinites, the antigorites are aligned parallel to each other forming schistose texture (Fig. 2B). The Cr-spinel grains are commonly zoned, composed of fresh cores surrounded by ferritchromite and/or chromian magnetite alteration zones (Figs. 2C & D). The sizes of the different zones vary from grain to another and the fresh Cr-spinel is sometimes present as isolated segments (Fig. 2C) or relics within ferritchromite and/or chromian magnetite. Magnetite occurs as fine disseminations and streaks. Carbonate grains and patches are interstitial to serpentine. They vary in abundance within the same sample and are more abundant in the foliated serpentinite (Fig. 2E). Carbonates are also present as veinlets in the foliated serpentinites. The talc-carbonate rock (Fig. 2F) is composed of talc, carbonates and chlorite with relics of serpentine.

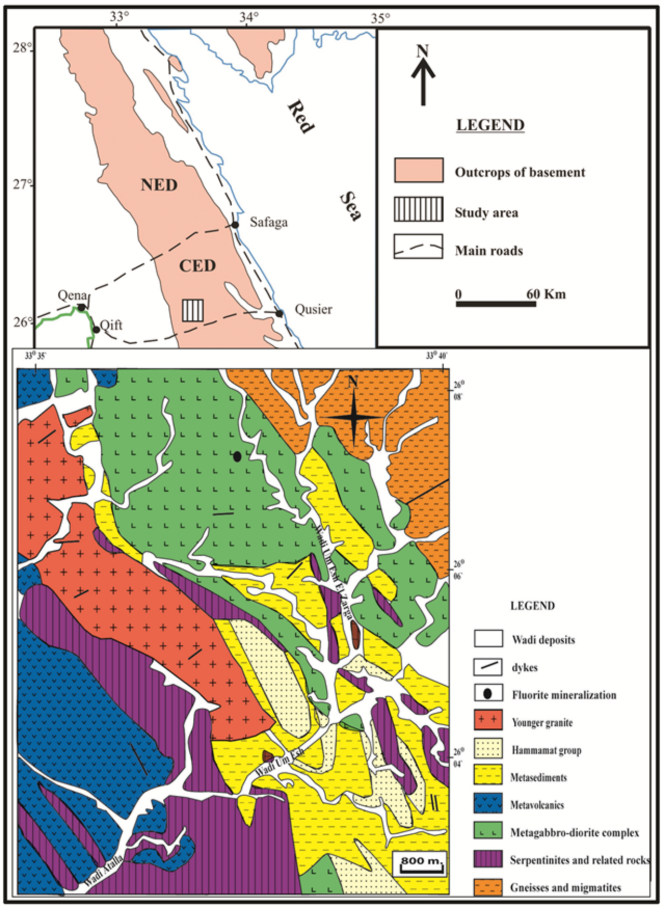

Fig. 1: Location and geologic map of Um Esh area (modified after Wassef et al., 1973), Central Eastern Desert (CED), Egypt. NED: North Eastern Desert.

ANALYTICAL TECHNIQUES

Whole-rock analyses were performed using wave-length dispersive X-ray fluorescence spectrometer (WD-XRF, Axios, PANalytical). Minerals were analyzed using a JEOL JXA-8200 electron probe microanalyzer equipped with five wavelength dispersive spectrometers (WDS). The whole-rock and electron microprobe analyses were carried out at the Institute of Geochemistry and Petrology, ETH-Zurich, Switzerland. The description and detection limits of the methods used in minerals and whole-rock analyses are given in Basta et al. (2011, 2017).

MINERAL CHEMISTRY

Unfortunately, the mantle peridotites of Um Esh area were extensively serpentinized and the primary silicate minerals are completely obliterated in the examined samples. However, fresh relics of primary Cr-spinels survived the serpentinization and metamorphism. Thus, the minerals analyses were restricted to fresh cores and altered zones of Cr-spinel, serpentine minerals and carbonates.

Cr-Spinel

The Cr-spinel grains of Um Esh serpentinites are usually zoned, with fresh cores or relics surrounded by metamorphic (ferritchromite and chromian magnetite) zones. The microprobe analyses of the different zones either as individual spots or profiles from fresh Cr-spinel to metamorphic spinels are given Tables 1 and 2. The fresh cores of Cr-spinel grains of massive and foliated serpentinites have similar composition. On average, the fresh Cr-spinels of massive serpentinites have slightly higher Cr_2O_3 (48.22 wt%), MgO (10.27 wt%), MnO (1.48 wt%), Cr# (61.82) and Mg# (50.64) compared with those of the foliated serpentinites (Cr_2O_3 = 44.39 wt%, MgO = 9.81 wt%, MnO = 0.78 wt%, Cr# = 55.25, Mg# = 46.34). On the other hand, they have slightly lower Al_2O_3 (20.02 wt%), FeO (19.09 wt%) and NiO (0.02 wt%) values than those of Cr-spinels of the foliated varieties (Al_2O_3 = 24.13 wt%, FeO = 21.15 wt %, NiO = 0.06 wt%). The Cr_2O_3 and Al_2O_3 abundances of the fresh Cr-spinels are similar to those of mantle spinels and Cr-spinels of the ophiolites of the Arabian-Nubian Shield (Fig. 3).

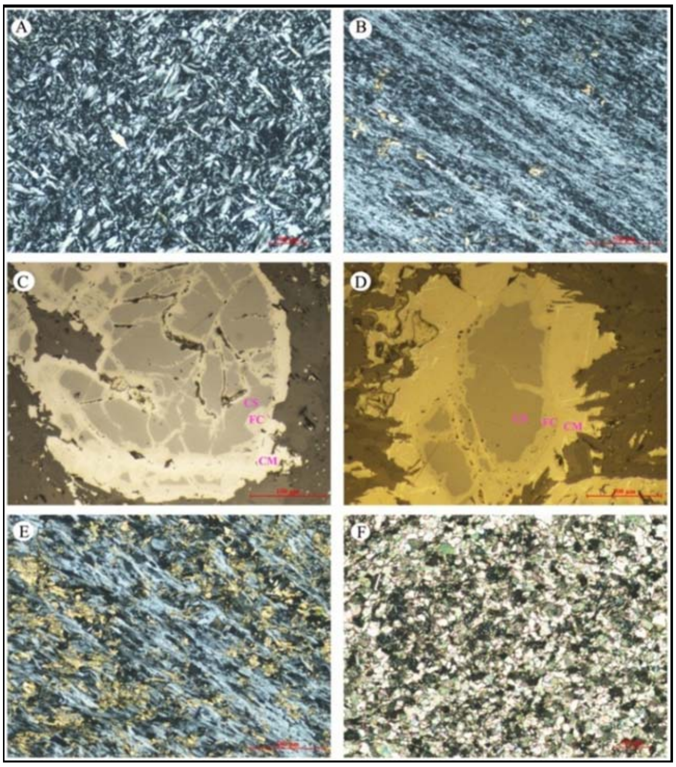

Fig. 2. Petrography of Um Esh serpentinites. (A) Massive antigorite serpentinite, (B) foliated antigorite serpentinite, (C) and (D) Zoned Cr-spinel in massive and foliated serpentinites, respectively, (E) Magnesite aggregates in foliated serpentinite, (F) Talc-carbonate rock with relict serpentine and chlorite. CS, fresh Cr-spinel; FC, ferritchromite; CM, chromian magnetite.

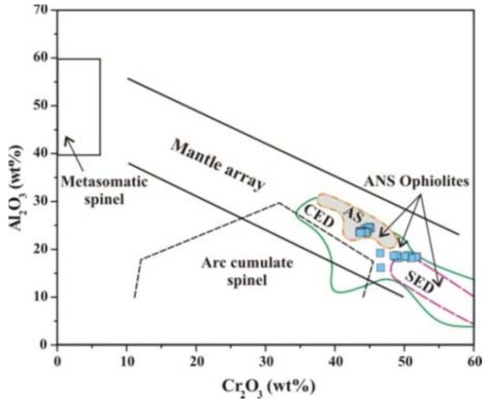

Fig. 3: Al_2O_3 versus Cr_2O_3 diagram (after Franz and Wirth, 2000) for Cr-spinels of Um Esh serpentinites. Data sources of Cr-spinel of Arabian-Nubian Shield (ANS) ophiolites are Ahmed (2013) and Ahmed et al. (2001, 2012). CED, Central Eastern Desert; SED, South Eastern Desert; AS, Arabian Shield.

The variation of Cr_2O_3, Al_2O_3, MgO, FeO, MnO and NiO abundances and Fe# (Fe^{3+}/Cr+Al+Fe^{3+}) along 4 profiles in 4 Cr-spinel grains (3 in massive serpentinites and 1 in foliated serpentinites, Table 2) from fresh cores through ferritchromite zones (best developed in profile #4) to chromian magnetite zones is shown in Figure 4. These profiles reveal that Al_2O_3 and MgO abundances rapidly dropped from the fresh Cr-spinel to the ferritchromite zones then markedly decreased towards the chromian magnetite zones or rims (Fig. 4A and B). The Cr_2O_3 contents show slight to moderate decrease from fresh Cr-spinel to the ferritchromite then another significant decrease in the chromian magnetite. Within the individual ferritchromite and chromian magnetite zones the Cr_2O_3 contents show gradual decrease. On the other hand, these profiles show that FeO abundances and Fe# rapidly increased from the fresh Cr-spinel to the ferritchromite zones then significantly increased again in the chromian magnetite (Fig. 4C and D). Contrary to the other elements, the behaviour of MnO and NiO was not uniform (Fig. 4E and F). MnO contents increase from fresh Cr-spinel to ferritchromite then decrease in the chromian magnetite (Fig. 4E), while the NiO contents increase from the fresh Cr-spinel through the ferritchromite to the inner zone of chromian magnetite then decrease in the outer rim of chromian magnetite zone (Fig. 4F).

Serpentine

The composition of serpentines of the Um Esh serpentinites is given in Table 3. The serpentines of the massive and foliated serpentinites have low Al_2O_3 abundances (average = 0.62 and 0.58 wt%, respectively). The serpentine of massive serpentinite has SiO_2 (42.18-44.42 wt%, average = 43.56 wt%), MgO (38.8-41.7 wt%, average = 40.10 wt%) and FeO (1.72-4.18 wt%, average = 2.46 wt%) abundances which are comparable to those of serpentines of foliated varieties (SiO_2 = 43.10-44.75 wt%, average = 43.80 wt%; MgO = 37.22-40.55 wt%, average = 39.57 wt%; FeO = 2.49-3.37 wt%, average = 2.85 wt%). These serpentines contain some Cr (Cr_2O_3<0.36 wt%) and NiO (up to 0.91 wt%). Plotting the analyzed serpentines on the Al_2O_3 versus SiO_2 diagram (Schwartz et al., 2013) suggests that they are essentially antigorites with few lizardites (Fig. 5). The relatively high SiO_2 contents (42.18-44.75 wt%; average = 43.65 wt%) of serpentines of Um Esh serpentinites, together with MgO values greater than 37 wt%, indicate that they are antigorites rather than lizardites (Dungan, 1979). XRD results of serpentinite samples from the northwestern tip of this ultramafic belt near Atalla gold mine confirm that the serpentine minerals are dominated by antigorite (Bakhit, 1994).

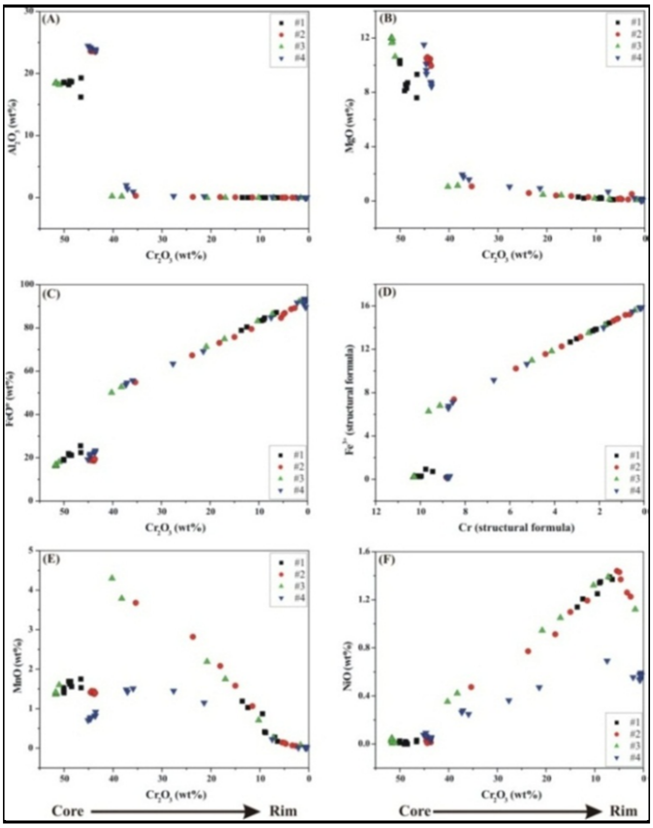

Fig. 4: Profiles along zoned Cr-spinels showing compositional variations of different zones.

Carbonate

The microprobe analysis of the carbonates of massive and foliated serpentinites is given in Table 4. The chemical composition of these carbonates reveals that they are magnesites. However, the magnesites of the massive serpentinites have slightly higher FeO contents (0.89-1.96 wt%) and lower CaO (0.04-0.18 wt%) and MnO (0.33-0.43 wt%) contents compared with those of the foliated serpentinites (FeO = 1.26-1.52 wt%, CaO = 0.23-0.86 wt%, MnO = 0.51-0.66 wt%).

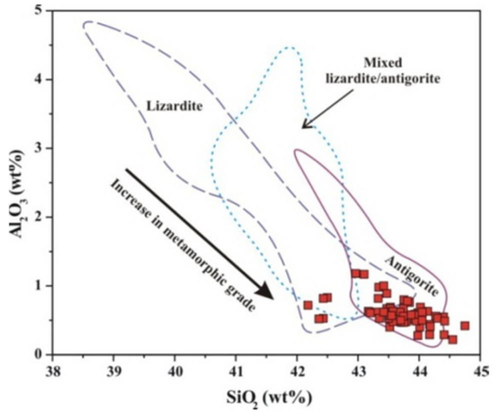

Fig. 5. Al_2O_3 versus SiO_2 diagram (after Schwartz et al., 2013) for the serpentines of Um Esh serpentinites.

WHOLE-ROCK GEOCHEMISTRY

Whole-rock chemical composition of 8 massive and foliated serpentinite samples is given in Table 5. The massive and foliated serpentinites have similar elements abundances (Table 5). The analyzed samples have high MgO contents (37.06-39.24 wt%) and Mg# (90.6-91.8), and low Al_2O_3 (0.37-0.71 wt%) and CaO (0-3.32 wt%) contents. The generally low CaO in the analyzed serpentinites reflect low clinopyroxene abundance in the original peridotites. The high CaO abundances in some samples are attributed to the presence of secondary carbonates. The analyzed samples are largely classified as harzburgites using the normative proportions of olivine, orthopyroxene and clinopyroxene (Fig. 6), suggesting harzburgite protolith. Samples with secondary carbonates plot in the dunite and wehrlite fields. The Um Esh serpentinites have MgO/SiO_2 (0.96-1.11) and low Al_2O_3/SiO_2 (0.010-0.016) values comparable to those of fore-arc peridotites (Fig. 7), suggesting that they represent residual mantle rocks which have experienced high degree of partial melting. On average, the analyzed serpentinites have Ni content (2540 ppm) higher than and Cr content (3002 ppm) lower than that of primitive mantle (Ni = 2090 ppm; Cr = 3240 ppm, Hart and Zindler, 1986).

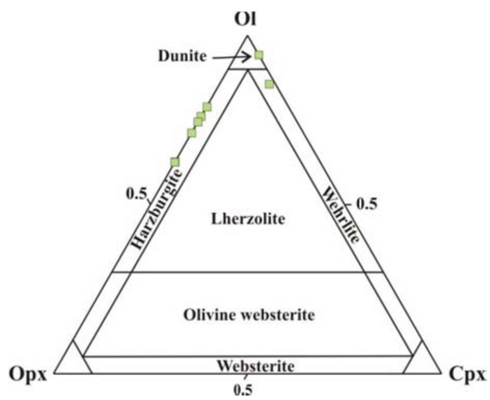

Fig. 6: Nomenclature of the Um Esh serpentinites based on Ol-Opx-Cpx normative composition (after Coleman, 1977).

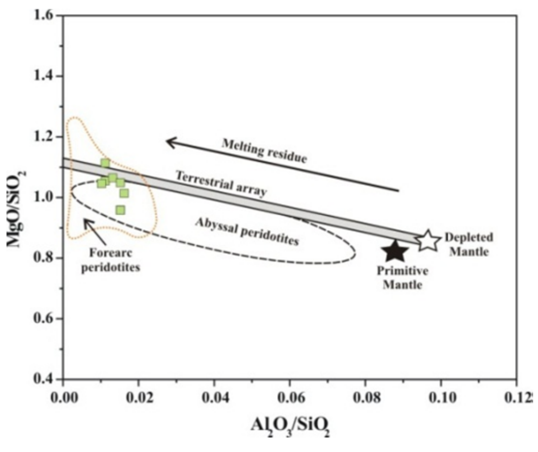

Fig. 7: MgO/SiO_2 versus Al_2O_3/SiO_2 diagram for the Um Esh serpentinites. Terrestrial array after Jagoutz et al. (1979) and Hart and Zindler (1986). Abyssal peridotites field after Niu (2004), the forearc peridotites (South Sandwich and Izu-Bonin-Mariana) field after Pearce et al. (2000) and Parkinson and Pearce (1998).

Table 1. Representative microprobe analyses of Cr-spinel of Um Esh serpentinites, Eastern Desert, Egypt.

	Massive serpentinite										**Foliated serpentinite**								
	Fresh Cr-spinel						Altered spinel				Fresh Cr-spinel					Altered spinel			
No.	1	2	3	4	5	6	7	8	9	10	11	12	13	14	15	16	17	18	19
SiO_2	0.000	0.000	0.000	0.000	0.009	0.000	0.000	0.000	0.000	0.000	0.013	0.000	0.000	0.000	0.010	0.000	0.000	1.306	0.000
TiO_2	0.002	0.001	0.000	0.000	0.001	0.000	0.003	0.000	0.006	0.013	0.013	0.010	0.016	0.000	0.000	0.010	0.016	0.016	0.000
Al_2O_3	18.830	18.460	19.280	23.700	23.610	23.590	0.117	0.000	0.000	24.730	24.370	24.530	23.910	23.660	23.760	9.140	1.614	1.606	0.000
Cr_2O_3	50.520	51.790	46.540	44.630	43.910	44.340	22.990	9.290	6.580	45.020	44.650	44.820	44.250	44.040	43.970	38.980	36.580	26.780	0.563
FeO	18.610	16.190	22.400	18.550	19.380	18.990	67.350	83.620	84.290	18.880	20.550	19.350	22.420	22.340	22.530	44.030	54.320	62.020	92.980
MnO	1.470	1.360	1.530	1.380	1.440	1.430	2.660	0.495	0.281	0.711	0.762	0.694	0.854	0.857	0.860	1.271	1.500	1.034	0.011
MgO	10.330	12.030	9.320	10.800	10.120	10.350	0.564	0.267	0.175	11.650	10.340	11.500	8.760	8.630	8.330	3.940	1.800	3.600	0.179
NiO	0.013	0.028	0.031	0.018	0.031	0.051	0.850	1.350	1.450	0.065	0.061	0.066	0.037	0.054	0.044	0.208	0.261	0.394	0.572
Total	99.77	99.86	99.11	99.08	98.51	98.76	94.53	95.05	92.80	101.08	100.76	100.97	100.25	99.59	99.51	97.59	96.11	96.76	94.31
Formula based on 32 oxygens																			
Si	0.000	0.000	0.000	0.000	0.002	0.000	0.000	0.000	0.000	0.000	0.003	0.000	0.000	0.000	0.003	0.000	0.000	0.380	0.000
Ti	0.000	0.000	0.000	0.000	0.000	0.000	0.001	0.000	0.002	0.002	0.002	0.002	0.003	0.000	0.000	0.002	0.004	0.003	0.000
Al	5.645	5.477	5.836	6.983	7.025	6.995	0.042	0.000	0.000	7.100	7.085	7.061	7.066	7.046	7.091	3.028	0.569	0.551	0.000
Cr	10.161	10.309	9.450	8.821	8.764	8.821	5.612	2.257	1.638	8.671	8.708	8.654	8.772	8.798	8.803	8.663	8.651	6.160	0.136
Fe^{3+}	0.193	0.214	0.714	0.197	0.207	0.184	10.344	13.743	14.359	0.224	0.196	0.281	0.156	0.156	0.100	4.305	6.773	8.522	15.864
Fe^{2+}	3.766	3.195	4.097	3.681	3.884	3.812	7.046	7.741	7.839	3.622	4.043	3.671	4.545	4.564	4.671	6.045	6.814	6.567	7.914
Mn	0.317	0.290	0.333	0.292	0.308	0.305	0.696	0.129	0.075	0.147	0.159	0.144	0.181	0.183	0.185	0.302	0.380	0.255	0.003
Mg	3.918	4.515	3.569	4.025	3.809	3.883	0.259	0.122	0.082	4.231	3.803	4.187	3.275	3.251	3.145	1.651	0.803	1.562	0.082
Total	24	24	24	24	24	24	24	24	24	24	24	24	24	24	24	24	24	24	24
Cr#	0.64	0.65	0.62	0.56	0.56	0.56	0.99	1.00	1.00	0.55	0.55	0.55	0.55	0.56	0.55	0.74	0.94	0.92	1.00
Mg#	0.51	0.59	0.47	0.52	0.50	0.50	0.04	0.02	0.01	0.54	0.48	0.53	0.42	0.42	0.40	0.21	0.11	0.19	0.01
Fe#	0.01	0.01	0.04	0.01	0.01	0.01	0.65	0.86	0.90	0.01	0.01	0.02	0.01	0.01	0.01	0.27	0.42	0.56	0.99

Table 2: Composition and structural formula along 4 traverses in zoned Cr-spinel of Um Esh serpentinites, Eastern Desert, Egypt.

Massive serpentinite																	
	Traverse1																
	Fresh Cr-spinel		Altered spinel														
No.	1	2	3	4	5	6	7	8	9	10	11	12	13	14	15	16	17
SiO_2	0.000	0.000	0.000	0.000	0.000	0.000	0.000	0.446	0.000	0.000	0.000	0.013	0.000	0.026	0.000	0.000	0.000
TiO_2	0.003	0.005	0.000	0.013	0.004	0.009	0.007	0.002	0.022	0.000	0.000	0.000	0.000	0.004	0.000	0.005	0.012
Al_2O_3	18.530	18.510	18.500	18.610	18.190	18.590	18.790	16.210	18.700	19.280	0.000	0.000	0.000	0.026	0.018	0.000	0.000
Cr_2O_3	50.020	50.110	50.110	50.040	49.080	48.660	48.870	46.600	48.470	46.540	9.030	6.410	8.830	13.600	12.460	6.970	9.450
FeO	18.830	18.990	19.030	19.310	21.900	21.360	21.160	25.550	21.110	22.400	83.760	87.140	84.630	78.890	80.420	86.350	83.390
MnO	1.400	1.440	1.530	1.480	1.690	1.690	1.620	1.750	1.560	1.530	0.413	0.173	0.396	1.188	1.031	0.280	0.870
MgO	10.340	10.300	10.260	10.110	8.120	8.300	8.570	7.600	8.700	9.320	0.254	0.105	0.186	0.296	0.206	0.112	0.173
NiO	0.020	0.011	0.010	0.025	0.000	0.012	0.020	0.019	0.000	0.031	1.340	1.370	1.350	1.139	1.207	1.390	1.250
Total	99.14	99.37	99.44	99.59	98.98	98.62	99.04	98.18	98.56	99.10	94.80	95.21	95.39	95.17	95.34	95.11	95.14
Formula based on 32 oxygens																	
Si	0.000	0.000	0.000	0.000	0.000	0.000	0.000	0.118	0.000	0.000	0.000	0.004	0.000	0.008	0.000	0.000	0.000
Ti	0.001	0.001	0.000	0.002	0.001	0.002	0.001	0.000	0.004	0.000	0.000	0.000	0.000	0.001	0.000	0.001	0.003
Al	5.591	5.575	5.571	5.600	5.587	5.712	5.738	5.062	5.728	5.836	0.000	0.000	0.000	0.010	0.007	0.000	0.000
Cr	10.125	10.125	10.123	10.101	10.112	10.030	10.011	9.762	9.961	9.450	2.199	1.554	2.138	3.298	3.019	1.693	2.293
Fe^{3+}	0.283	0.298	0.306	0.294	0.300	0.255	0.249	0.939	0.302	0.714	13.801	14.438	13.862	12.675	12.974	14.305	13.702
Fe^{2+}	3.748	3.761	3.760	3.829	4.473	4.402	4.335	4.723	4.286	4.097	7.773	7.910	7.812	7.560	7.638	7.877	7.696
Mn	0.304	0.312	0.331	0.320	0.373	0.373	0.355	0.393	0.343	0.333	0.108	0.045	0.103	0.309	0.268	0.073	0.226
Mg	3.947	3.925	3.909	3.849	3.155	3.226	3.310	3.002	3.371	3.569	0.117	0.048	0.085	0.135	0.094	0.051	0.079
Total	24	24	24	24	24	24	24	24	24	24	24	24	24	24	24	24	24
Cr#	0.64	0.64	0.65	0.64	0.64	0.64	0.64	0.66	0.63	0.62	1.00	1.00	1.00	1.00	1.00	1.00	1.00
Mg#	0.51	0.51	0.51	0.50	0.41	0.42	0.43	0.39	0.44	0.47	0.01	0.01	0.01	0.02	0.01	0.01	0.01
Fe#	0.02	0.02	0.02	0.02	0.02	0.02	0.02	0.06	0.02	0.04	0.86	0.90	0.87	0.79	0.81	0.89	0.86

Table 2. Cont.

Massive serpentinite																	
	Traverse2																
	Fresh Cr-spinel		Altered spinel														
No.	1	2	3	4	5	6	7	8	9	10	11	12	13	14	15	16	17
SiO_2	0.000	0.014	0.034	0.007	0.000	0.009	0.009	0.030	0.000	0.000	0.053	0.000	0.007	0.000	0.003	0.000	0.226
TiO_2	0.000	0.001	0.002	0.012	0.000	0.001	0.005	0.006	0.003	0.000	0.000	0.003	0.000	0.014	0.004	0.000	0.002
Al_2O_3	23.590	23.620	23.580	23.590	23.590	23.610	23.490	0.291	0.108	0.092	0.050	0.032	0.000	0.000	0.000	0.000	0.000
Cr_2O_3	44.340	43.850	44.400	44.600	44.380	43.910	43.650	35.360	23.690	18.110	15.010	11.530	4.690	5.440	4.970	3.390	2.640
FeO	18.990	18.520	18.770	18.880	19.000	19.380	19.410	54.870	67.370	73.110	75.850	79.500	86.910	84.660	86.300	88.670	89.210
MnO	1.430	1.370	1.400	1.410	1.450	1.440	1.400	3.680	2.820	2.080	1.580	1.065	0.111	0.143	0.134	0.070	0.056
MgO	10.350	10.460	10.600	10.510	10.290	10.120	9.950	1.080	0.587	0.401	0.360	0.280	0.134	0.138	0.186	0.116	0.511
NiO	0.051	0.033	0.009	0.027	0.008	0.031	0.014	0.474	0.772	0.913	1.098	1.194	1.370	1.440	1.430	1.260	1.226
Total	98.75	97.87	98.79	99.04	98.72	98.50	97.93	95.79	95.35	94.71	94.00	93.60	93.22	91.83	93.03	93.51	93.87
Formula based on 32 oxygens																	
Si	0.000	0.003	0.008	0.002	0.000	0.002	0.002	0.009	0.000	0.000	0.016	0.000	0.002	0.000	0.001	0.000	0.070
Ti	0.000	0.000	0.000	0.002	0.000	0.000	0.001	0.001	0.001	0.000	0.000	0.001	0.000	0.003	0.001	0.000	0.001
Al	6.995	7.049	6.976	6.970	6.998	7.025	7.034	0.104	0.039	0.034	0.018	0.012	0.000	0.000	0.000	0.000	0.000
Cr	8.821	8.779	8.811	8.840	8.831	8.764	8.768	8.499	5.729	4.410	3.685	2.843	1.160	1.368	1.233	0.835	0.644
Fe^{3+}	0.184	0.165	0.196	0.182	0.171	0.207	0.191	7.376	10.231	11.557	12.264	13.144	14.835	14.625	14.764	15.165	15.215
Fe^{2+}	3.812	3.757	3.744	3.776	3.828	3.884	3.933	6.574	7.002	7.274	7.432	7.588	7.906	7.895	7.875	7.923	7.820
Mn	0.305	0.294	0.298	0.299	0.309	0.308	0.301	0.948	0.731	0.543	0.416	0.281	0.029	0.038	0.036	0.018	0.015
Mg	3.883	3.949	3.967	3.928	3.861	3.809	3.769	0.490	0.268	0.184	0.167	0.130	0.062	0.065	0.087	0.054	0.235
Total	24	24	24	24	24	24	24	24	24	24	24	24	24	24	24	24	24
Cr#	0.56	0.55	0.56	0.56	0.56	0.56	0.55	0.99	0.99	0.99	1.00	1.00	1.00	1.00	1.00	1.00	1.00
Mg#	0.50	0.51	0.51	0.51	0.50	0.50	0.49	0.07	0.04	0.02	0.02	0.02	0.01	0.01	0.01	0.01	0.03
Fe#	0.01	0.01	0.01	0.01	0.01	0.01	0.01	0.46	0.64	0.72	0.77	0.82	0.93	0.91	0.92	0.95	0.96

Table 2. Cont.

Massive serpentinite														
	Traverse3													
	Fresh Cr-spinel							Altered spinel						
No.	1	2	3	4	5	6	7	8	9	10	11	12	13	14
SiO_2	0.000	0.000	0.027	0.000	0.000	0.000	0.000	0.000	0.000	0.058	0.000	0.000	0.000	0.000
TiO_2	0.000	0.000	0.020	0.001	0.000	0.000	0.001	0.006	0.002	0.014	0.000	0.005	0.015	0.000
Al_2O_3	18.410	18.450	18.460	18.460	18.510	18.430	18.200	0.000	0.000	0.001	0.000	0.200	0.210	0.000
Cr_2O_3	51.560	51.730	51.640	51.790	51.590	51.710	51.010	7.190	10.250	17.050	20.790	38.220	40.210	1.680
FeO	16.620	16.140	16.290	16.190	16.460	16.920	18.030	86.540	83.150	74.930	71.350	52.730	50.140	92.290
MnO	1.380	1.370	1.390	1.360	1.390	1.420	1.600	0.271	0.709	1.750	2.190	3.790	4.300	0.078
MgO	11.750	12.000	12.010	12.030	11.970	11.640	10.630	0.140	0.196	0.420	0.466	1.131	1.058	0.073
NiO	0.006	0.032	0.050	0.028	0.018	0.045	0.010	1.390	1.320	1.050	0.945	0.422	0.353	1.121
Total	99.73	99.72	99.89	99.86	99.94	100.16	99.48	95.54	95.63	95.27	95.74	96.50	96.29	95.24
	Formula based on 32 oxygens													
Si	0.000	0.000	0.007	0.000	0.000	0.000	0.000	0.000	0.000	0.018	0.000	0.000	0.000	0.000
Ti	0.000	0.000	0.004	0.000	0.000	0.000	0.000	0.001	0.000	0.003	0.000	0.001	0.003	0.000
Al	5.479	5.482	5.477	5.477	5.488	5.469	5.473	0.000	0.000	0.001	0.000	0.071	0.075	0.000
Cr	10.293	10.311	10.278	10.309	10.261	10.294	10.290	1.738	2.476	4.130	5.016	9.128	9.634	0.405
Fe^{3+}	0.228	0.206	0.225	0.214	0.252	0.237	0.238	14.259	13.523	11.827	10.984	6.799	6.284	15.595
Fe^{2+}	3.281	3.196	3.204	3.195	3.211	3.326	3.609	7.864	7.724	7.371	7.222	6.520	6.422	7.947
Mn	0.295	0.293	0.296	0.290	0.296	0.303	0.346	0.070	0.184	0.454	0.566	0.970	1.104	0.020
Mg	4.423	4.511	4.507	4.515	4.489	4.370	4.043	0.064	0.089	0.192	0.212	0.509	0.478	0.033
Total	24	24	24	24	24	24	24	24	24	24	24	24	24	24
Cr#	0.65	0.65	0.65	0.65	0.65	0.65	0.65	1.00	1.00	1.00	1.00	0.99	0.99	1.00
Mg#	0.57	0.59	0.58	0.59	0.58	0.57	0.53	0.01	0.01	0.03	0.03	0.07	0.07	0.00
Fe#	0.01	0.01	0.01	0.01	0.02	0.01	0.01	0.89	0.85	0.74	0.69	0.43	0.39	0.97

Table 2. Cont.

	Foliated serpentinite																				
	Traverse4																				
	Fresh Cr-spinel							Altered spinel													
No.	1	2	3	4	5	6	7	8	9	10	11	12	13	14	15	16	17	18	19	20	21
SiO_2	0.009	0.000	0.000	0.000	0.000	0.014	0.000	0.012	0.003	0.000	0.047	0.061	0.282	0.000	0.001	0.000	0.000	0.018	0.000	0.000	0.052
TiO_2	0.013	0.009	0.005	0.024	0.004	0.015	0.018	0.007	0.019	0.008	0.018	0.009	0.007	0.000	0.006	0.000	0.000	0.003	0.000	0.014	0.000
Al_2O_3	24.450	24.210	23.980	23.890	23.890	23.850	23.580	1.980	1.389	0.945	0.229	0.199	0.095	0.000	0.000	0.000	0.000	0.011	0.000	0.000	0.000
Cr_2O_3	45.100	44.660	44.620	44.600	43.710	43.590	43.560	37.290	37.050	35.900	27.620	21.400	7.470	2.130	0.680	0.573	0.592	0.521	0.759	0.784	0.402
FeO	19.200	20.730	20.970	21.730	22.410	22.500	23.330	53.710	54.640	55.680	63.450	69.170	84.750	91.630	93.340	93.460	92.710	91.730	90.780	92.320	89.460
MnO	0.705	0.745	0.735	0.781	0.824	0.820	0.916	1.480	1.420	1.510	1.450	1.150	0.224	0.009	0.018	0.028	0.005	0.033	0.029	0.018	0.007
MgO	11.510	10.090	9.630	9.350	8.760	8.610	8.420	1.940	1.760	1.573	1.048	0.935	0.680	0.206	0.162	0.138	0.117	0.087	0.024	0.031	0.042
NiO	0.075	0.092	0.066	0.065	0.028	0.047	0.056	0.263	0.278	0.248	0.362	0.471	0.692	0.555	0.533	0.581	0.540	0.592	0.574	0.532	0.571
Total	101.06	100.54	100.01	100.44	99.63	99.45	99.88	96.68	96.56	95.86	94.22	93.39	94.20	94.53	94.74	94.78	93.96	92.99	92.17	93.70	90.53
Formula based on 32 oxygens																					
Si	0.002	0.000	0.000	0.000	0.000	0.003	0.000	0.003	0.001	0.000	0.014	0.019	0.086	0.000	0.000	0.000	0.000	0.006	0.000	0.000	0.017
Ti	0.002	0.002	0.001	0.004	0.001	0.003	0.003	0.001	0.004	0.002	0.004	0.002	0.002	0.000	0.001	0.000	0.000	0.001	0.000	0.003	0.000
Al	7.035	7.069	7.061	7.023	7.097	7.105	7.014	0.692	0.488	0.335	0.083	0.073	0.034	0.000	0.000	0.000	0.000	0.004	0.000	0.000	0.000
Cr	8.705	8.748	8.813	8.796	8.711	8.712	8.692	8.746	8.736	8.547	6.716	5.243	1.808	0.514	0.164	0.138	0.144	0.128	0.188	0.191	0.101
Fe^{3+}	0.251	0.180	0.124	0.172	0.191	0.170	0.287	6.551	6.766	7.114	9.164	10.642	13.981	15.486	15.833	15.862	15.856	15.855	15.812	15.803	15.865
Fe^{2+}	3.668	4.115	4.257	4.361	4.533	4.586	4.637	6.773	6.860	6.908	7.154	7.283	7.719	7.902	7.924	7.926	7.944	7.957	7.977	7.979	7.986
Mn	0.146	0.156	0.156	0.165	0.176	0.175	0.196	0.372	0.359	0.385	0.378	0.302	0.058	0.002	0.005	0.007	0.001	0.009	0.008	0.005	0.002
Mg	4.189	3.727	3.587	3.477	3.292	3.245	3.168	0.858	0.783	0.706	0.480	0.432	0.311	0.094	0.073	0.063	0.053	0.040	0.011	0.014	0.020
Total	24	24	24	24	24	24	24	24	24	24	24	24	24	24	24	24	24	24	24	24	24
Cr#	0.55	0.55	0.56	0.56	0.55	0.55	0.55	0.93	0.95	0.96	0.99	0.99	0.98	1.00	1.00	1.00	1.00	0.97	1.00	1.00	1.00
Mg#	0.53	0.48	0.46	0.44	0.42	0.41	0.41	0.11	0.10	0.09	0.06	0.06	0.04	0.01	0.01	0.01	0.01	0.01	0.00	0.00	0.00
Fe#	0.02	0.01	0.01	0.01	0.01	0.01	0.02	0.41	0.42	0.44	0.57	0.67	0.88	0.97	0.99	0.99	0.99	0.99	0.99	0.99	0.99

Table 3. Composition and structural formula of serpentines of Um Esh serpentinites, Eastern Desert, Egypt.

	Massive serpentinite																				
No.	1	2	3	4	5	6	7	8	9	10	11	12	13	14	15	16	17	18	19	20	21
SiO_2	43.420	43.710	43.170	42.430	43.440	44.170	43.500	42.960	42.360	43.350	43.720	43.750	43.950	43.930	44.020	44.140	43.690	44.050	44.400	43.570	43.520
TiO_2	0.000	0.000	0.000	0.000	0.000	0.000	0.000	0.011	0.000	0.000	0.000	0.000	0.000	0.000	0.000	0.000	0.000	0.000	0.000	0.000	0.000
Al_2O_3	1.004	0.465	0.632	0.530	0.615	0.290	0.529	1.179	0.520	0.531	0.502	0.466	0.492	0.590	0.686	0.632	0.620	0.619	0.551	0.634	0.570
FeO	2.290	1.970	2.510	2.290	2.130	1.720	2.060	2.430	3.810	2.210	2.000	1.810	2.020	2.330	2.450	2.720	2.840	2.870	2.050	2.120	2.090
MnO	0.016	0.042	0.038	0.052	0.034	0.043	0.023	0.035	0.054	0.030	0.028	0.053	0.032	0.054	0.059	0.047	0.055	0.034	0.029	0.050	0.052
MgO	40.260	40.310	39.550	40.320	40.230	40.780	39.900	40.130	39.200	39.770	40.970	41.130	40.830	40.070	39.410	39.320	39.380	40.030	41.700	40.440	40.500
CaO	0.006	0.012	0.000	0.013	0.000	0.013	0.000	0.000	0.014	0.011	0.000	0.005	0.000	0.000	0.011	0.007	0.019	0.000	0.003	0.007	0.005
Na_2O	0.000	0.000	0.000	0.000	0.013	0.000	0.000	0.020	0.017	0.000	0.000	0.002	0.000	0.000	0.009	0.000	0.000	0.000	0.000	0.000	0.000
K_2O	0.001	0.000	0.006	0.008	0.004	0.000	0.005	0.008	0.012	0.001	0.000	0.000	0.000	0.000	0.008	0.004	0.003	0.006	0.005	0.000	0.000
Cr_2O_3	0.030	0.121	0.121	0.091	0.094	0.005	0.078	0.273	0.243	0.116	0.088	0.093	0.104	0.112	0.111	0.089	0.095	0.119	0.124	0.113	0.061
NiO	0.093	0.278	0.115	0.162	0.050	0.042	0.325	0.157	0.404	0.265	0.114	0.086	0.113	0.101	0.128	0.261	0.268	0.283	0.053	0.111	0.165
Total	87.12	86.91	86.14	85.89	86.61	87.06	86.42	87.20	86.63	86.28	87.42	87.39	87.54	87.19	86.89	87.22	86.97	88.01	88.91	87.04	86.96
Formula based on 9 oxygens																					
Si	2.593	2.616	2.611	2.578	2.608	2.630	2.619	2.571	2.577	2.616	2.601	2.601	2.610	2.621	2.635	2.637	2.622	2.614	2.597	2.604	2.604
Al	0.071	0.033	0.045	0.038	0.044	0.020	0.037	0.083	0.037	0.038	0.035	0.033	0.034	0.041	0.048	0.045	0.044	0.043	0.038	0.045	0.040
Ti	0.000	0.000	0.000	0.000	0.000	0.000	0.000	0.001	0.000	0.000	0.000	0.000	0.000	0.000	0.000	0.000	0.000	0.000	0.000	0.000	0.000
Fe	0.114	0.099	0.127	0.116	0.107	0.086	0.104	0.122	0.194	0.112	0.100	0.090	0.100	0.116	0.123	0.136	0.143	0.142	0.100	0.106	0.105
Mn	0.001	0.002	0.002	0.003	0.002	0.002	0.001	0.002	0.003	0.002	0.001	0.003	0.002	0.003	0.003	0.002	0.003	0.002	0.001	0.003	0.003
Mg	3.585	3.596	3.566	3.652	3.600	3.619	3.580	3.580	3.554	3.577	3.633	3.645	3.614	3.564	3.516	3.502	3.523	3.541	3.636	3.603	3.612
Ca	0.000	0.001	0.000	0.001	0.000	0.001	0.000	0.000	0.001	0.001	0.000	0.000	0.000	0.000	0.001	0.000	0.001	0.000	0.000	0.000	0.000
Na	0.000	0.000	0.000	0.000	0.002	0.000	0.000	0.002	0.002	0.000	0.000	0.000	0.000	0.000	0.001	0.000	0.000	0.000	0.000	0.000	0.000
K	0.000	0.000	0.000	0.001	0.000	0.000	0.000	0.001	0.001	0.000	0.000	0.000	0.000	0.000	0.001	0.000	0.000	0.000	0.000	0.000	0.000
Cr	0.001	0.006	0.006	0.004	0.004	0.000	0.004	0.013	0.012	0.006	0.004	0.004	0.005	0.005	0.005	0.004	0.004	0.006	0.006	0.005	0.003
Ni	0.004	0.013	0.006	0.008	0.002	0.002	0.016	0.008	0.020	0.013	0.005	0.004	0.005	0.005	0.006	0.013	0.013	0.014	0.002	0.005	0.008
Total	6.370	6.365	6.363	6.401	6.369	6.360	6.361	6.382	6.400	6.363	6.380	6.381	6.371	6.356	6.339	6.339	6.354	6.362	6.381	6.371	6.375

Table 3. Cont.

	Massive serpentinite															Foliated serpentinite					
No.	22	23	24	25	26	27	28	29	30	31	32	33	34	35	36	37	38	39	40	41	42
SiO_2	43.740	43.550	43.420	43.700	42.180	42.500	42.430	43.330	43.810	43.200	44.050	44.270	43.870	44.300	44.420	43.470	43.520	44.170	43.790	44.410	43.940
TiO_2	0.000	0.002	0.000	0.000	0.006	0.000	0.000	0.000	0.000	0.000	0.000	0.000	0.000	0.004	0.000	0.000	0.000	0.000	0.000	0.000	0.000
Al_2O_3	0.562	0.571	0.616	0.502	0.721	0.830	0.816	0.821	0.777	0.607	0.502	0.559	0.583	0.532	0.486	0.890	0.402	0.440	0.484	0.294	0.549
FeO	2.010	2.250	3.060	1.920	3.880	4.180	3.970	2.370	2.480	2.860	2.530	2.070	2.090	2.160	2.080	2.790	2.620	2.570	2.710	2.590	3.030
MnO	0.032	0.042	0.067	0.016	0.050	0.058	0.042	0.058	0.050	0.046	0.039	0.048	0.046	0.020	0.044	0.069	0.050	0.026	0.029	0.050	0.038
MgO	40.300	40.350	39.520	40.310	38.800	39.160	39.180	39.830	40.230	40.010	40.290	40.830	40.420	40.070	39.980	40.130	40.550	39.710	39.530	38.760	39.830
CaO	0.000	0.000	0.003	0.009	0.016	0.018	0.009	0.004	0.003	0.005	0.006	0.008	0.019	0.004	0.009	0.014	0.015	0.014	0.022	0.015	0.023
Na_2O	0.000	0.009	0.000	0.000	0.046	0.009	0.010	0.010	0.000	0.008	0.000	0.031	0.000	0.003	0.005	0.000	0.000	0.000	0.000	0.000	0.000
K_2O	0.002	0.000	0.005	0.000	0.025	0.022	0.013	0.015	0.006	0.004	0.002	0.008	0.009	0.006	0.005	0.002	0.000	0.002	0.004	0.000	0.004
Cr_2O_3	0.071	0.131	0.179	0.134	0.263	0.302	0.188	0.288	0.260	0.230	0.215	0.152	0.223	0.263	0.206	0.048	0.162	0.033	0.086	0.031	0.085
NiO	0.151	0.253	0.337	0.072	0.419	0.497	0.313	0.165	0.187	0.275	0.213	0.109	0.194	0.230	0.204	0.178	0.145	0.373	0.177	0.244	0.385
Total	86.87	87.16	87.21	86.66	86.41	87.57	86.97	86.89	87.80	87.25	87.85	88.09	87.45	87.59	87.44	87.59	87.46	87.34	86.83	86.39	87.88
Formula based on 9 oxygens																					
Si	2.616	2.603	2.606	2.618	2.574	2.564	2.570	2.600	2.602	2.591	2.615	2.613	2.610	2.630	2.639	2.592	2.598	2.635	2.629	2.672	2.615
Al	0.040	0.040	0.044	0.035	0.052	0.059	0.058	0.058	0.054	0.043	0.035	0.039	0.041	0.037	0.034	0.063	0.028	0.031	0.034	0.021	0.039
Ti	0.000	0.000	0.000	0.000	0.000	0.000	0.000	0.000	0.000	0.000	0.000	0.000	0.000	0.000	0.000	0.000	0.000	0.000	0.000	0.000	0.000
Fe	0.101	0.112	0.154	0.096	0.198	0.211	0.201	0.119	0.123	0.143	0.126	0.102	0.104	0.107	0.103	0.139	0.131	0.128	0.136	0.130	0.151
Mn	0.002	0.002	0.003	0.001	0.003	0.003	0.002	0.003	0.002	0.002	0.002	0.002	0.002	0.001	0.002	0.003	0.003	0.001	0.001	0.003	0.002
Mg	3.593	3.596	3.536	3.600	3.529	3.522	3.538	3.562	3.562	3.577	3.565	3.593	3.585	3.546	3.540	3.567	3.609	3.532	3.537	3.477	3.534
Ca	0.000	0.000	0.000	0.001	0.001	0.001	0.001	0.000	0.000	0.000	0.000	0.001	0.001	0.000	0.001	0.001	0.001	0.001	0.001	0.001	0.001
Na	0.000	0.001	0.000	0.000	0.005	0.001	0.001	0.001	0.000	0.001	0.000	0.004	0.000	0.000	0.001	0.000	0.000	0.000	0.000	0.000	0.000
K	0.000	0.000	0.000	0.000	0.002	0.002	0.001	0.001	0.000	0.000	0.000	0.001	0.001	0.000	0.000	0.000	0.000	0.000	0.000	0.000	0.000
Cr	0.003	0.006	0.008	0.006	0.013	0.014	0.009	0.014	0.012	0.011	0.010	0.007	0.010	0.012	0.010	0.002	0.008	0.002	0.004	0.001	0.004
Ni	0.007	0.012	0.016	0.003	0.021	0.024	0.015	0.008	0.009	0.013	0.010	0.005	0.009	0.011	0.010	0.009	0.007	0.018	0.009	0.012	0.018
Total	6.362	6.374	6.368	6.361	6.397	6.401	6.397	6.366	6.365	6.383	6.363	6.366	6.364	6.346	6.340	6.376	6.384	6.348	6.352	6.317	6.364

Table 3. Cont.

Foliated serpentinite																			
No.	43	44	45	46	47	48	49	50	51	52	53	54	55	56	57	58	59	60	61
SiO_2	43.920	44.750	44.550	43.980	43.470	43.530	43.840	43.740	43.570	43.300	43.500	43.750	43.590	43.340	43.530	44.180	43.980	44.010	43.100
TiO_2	0.000	0.000	0.002	0.000	0.000	0.000	0.000	0.005	0.000	0.003	0.000	0.000	0.000	0.001	0.000	0.000	0.000	0.000	0.000
Al_2O_3	0.505	0.421	0.216	0.277	0.668	0.693	0.756	0.675	0.480	0.622	0.570	0.804	0.634	0.977	0.667	0.409	0.605	0.400	1.172
FeO	2.690	2.720	2.620	2.820	2.930	2.760	3.220	3.100	2.810	3.370	2.970	3.010	3.360	2.860	3.000	2.490	2.790	2.510	2.970
MnO	0.047	0.050	0.053	0.022	0.015	0.042	0.010	0.074	0.010	0.037	0.022	0.025	0.040	0.035	0.030	0.032	0.046	0.015	0.041
MgO	39.590	38.950	37.220	39.910	40.080	40.070	38.910	38.670	39.670	39.510	39.530	39.310	39.260	40.170	39.650	40.500	39.570	40.400	39.810
CaO	0.016	0.028	0.003	0.015	0.013	0.021	0.040	0.031	0.015	0.012	0.015	0.012	0.010	0.018	0.010	0.011	0.014	0.011	0.007
Na_2O	0.000	0.000	0.000	0.000	0.000	0.006	0.000	0.000	0.005	0.008	0.000	0.000	0.004	0.000	0.000	0.000	0.000	0.002	0.011
K_2O	0.006	0.000	0.003	0.006	0.001	0.001	0.002	0.007	0.001	0.002	0.000	0.000	0.001	0.000	0.000	0.000	0.001	0.003	0.000
Cr_2O_3	0.088	0.053	0.017	0.003	0.075	0.037	0.076	0.063	0.040	0.160	0.195	0.164	0.200	0.363	0.261	0.005	0.157	0.019	0.145
NiO	0.335	0.272	0.210	0.163	0.132	0.139	0.739	0.907	0.242	0.418	0.243	0.256	0.305	0.201	0.269	0.190	0.247	0.128	0.257
Total	87.20	87.24	84.89	87.20	87.38	87.30	87.59	87.27	86.84	87.44	87.05	87.33	87.40	87.97	87.42	87.82	87.41	87.50	87.51
Formula based on 9 oxygens																			
Si	2.628	2.668	2.720	2.630	2.599	2.602	2.623	2.628	2.619	2.598	2.612	2.617	2.612	2.578	2.605	2.620	2.625	2.620	2.577
Al	0.036	0.030	0.016	0.020	0.047	0.049	0.053	0.048	0.034	0.044	0.040	0.057	0.045	0.069	0.047	0.029	0.043	0.028	0.083
Ti	0.000	0.000	0.000	0.000	0.000	0.000	0.000	0.000	0.000	0.000	0.000	0.000	0.000	0.000	0.000	0.000	0.000	0.000	0.000
Fe	0.135	0.136	0.134	0.141	0.146	0.138	0.161	0.156	0.141	0.169	0.149	0.151	0.168	0.142	0.150	0.124	0.139	0.125	0.149
Mn	0.002	0.003	0.003	0.001	0.001	0.002	0.001	0.004	0.000	0.002	0.001	0.001	0.002	0.002	0.002	0.002	0.002	0.001	0.002
Mg	3.531	3.462	3.388	3.558	3.572	3.571	3.470	3.463	3.554	3.534	3.538	3.505	3.508	3.561	3.537	3.581	3.521	3.585	3.548
Ca	0.001	0.002	0.000	0.001	0.001	0.001	0.003	0.002	0.001	0.001	0.001	0.001	0.001	0.001	0.001	0.001	0.001	0.001	0.000
Na	0.000	0.000	0.000	0.000	0.000	0.001	0.000	0.000	0.001	0.001	0.000	0.000	0.000	0.000	0.000	0.000	0.000	0.000	0.001
K	0.000	0.000	0.000	0.000	0.000	0.000	0.000	0.001	0.000	0.000	0.000	0.000	0.000	0.000	0.000	0.000	0.000	0.000	0.000
Cr	0.004	0.002	0.001	0.000	0.004	0.002	0.004	0.003	0.002	0.008	0.009	0.008	0.009	0.017	0.012	0.000	0.007	0.001	0.007
Ni	0.016	0.013	0.010	0.008	0.006	0.007	0.036	0.044	0.012	0.020	0.012	0.012	0.015	0.010	0.013	0.009	0.012	0.006	0.012
Total	6.353	6.316	6.272	6.360	6.376	6.373	6.349	6.347	6.364	6.377	6.363	6.351	6.361	6.380	6.366	6.365	6.350	6.366	6.379

Table 4. Composition of magnesite of Um Esh serpentinites, Eastern Desert, Egypt.

	Massive serpentinite														**Foliated serpentinite**		
No.	1	2	3	4	5	6	7	8	9	10	11	12	13	14	15	16	17	18
SiO_2	0.000	0.002	0.020	0.023	0.059	0.037	0.023	0.040	0.031	0.035	0.065	0.190	0.057	0.019	0.033	0.000	0.000	0.000
TiO_2	0.002	0.004	0.014	0.001	0.000	0.021	0.000	0.018	0.001	0.000	0.003	0.000	0.000	0.007	0.001	0.007	0.010	0.008
Al_2O_3	0.000	0.000	0.000	0.000	0.000	0.000	0.000	0.000	0.005	0.000	0.007	0.011	0.005	0.000	0.000	0.000	0.000	0.011
FeO	1.890	0.893	1.890	1.840	1.860	1.870	1.900	1.850	1.870	1.930	1.890	1.960	1.950	1.910	1.880	1.440	1.380	1.380
MnO	0.379	0.432	0.401	0.372	0.421	0.342	0.369	0.333	0.383	0.389	0.353	0.348	0.365	0.372	0.370	0.600	0.514	0.593
MgO	47.320	48.100	47.550	47.380	47.390	46.600	47.480	47.460	46.980	47.440	47.320	47.440	47.300	47.710	47.330	47.350	47.350	47.150
CaO	0.062	0.180	0.057	0.058	0.056	0.045	0.059	0.072	0.046	0.070	0.067	0.059	0.075	0.068	0.062	0.382	0.288	0.376
Na_2O	0.000	0.000	0.004	0.000	0.000	0.000	0.000	0.000	0.000	0.003	0.014	0.000	0.000	0.009	0.000	0.012	0.000	0.003
K_2O	0.000	0.000	0.003	0.000	0.000	0.000	0.000	0.003	0.004	0.000	0.000	0.000	0.000	0.001	0.004	0.001	0.000	0.002
NiO	0.031	0.015	0.029	0.031	0.044	0.036	0.043	0.033	0.033	0.033	0.030	0.047	0.034	0.018	0.048	0.019	0.038	0.009
Total	49.68	49.64	49.99	49.71	49.83	48.96	49.87	49.81	49.35	49.90	49.76	50.06	49.79	50.11	49.73	49.81	49.58	49.53

Table 4. Cont.

	Foliated serpentinite																
No.	19	20	21	22	23	24	25	26	27	28	29	30	31	32	33	34	35
SiO_2	0.000	0.000	0.000	0.006	0.000	0.001	0.000	0.000	0.000	0.000	0.004	0.030	0.000	0.000	0.001	0.000	0.000
TiO_2	0.000	0.005	0.000	0.002	0.000	0.005	0.000	0.001	0.009	0.000	0.000	0.000	0.008	0.010	0.004	0.002	0.001
Al_2O_3	0.000	0.000	0.000	0.000	0.000	0.000	0.000	0.000	0.000	0.000	0.000	0.002	0.013	0.003	0.000	0.015	0.012
FeO	1.490	1.520	1.480	1.390	1.450	1.310	1.300	1.420	1.450	1.360	1.460	1.410	1.360	1.272	1.262	1.330	1.286
MnO	0.628	0.662	0.585	0.537	0.570	0.512	0.510	0.603	0.601	0.544	0.655	0.580	0.588	0.559	0.558	0.581	0.550
MgO	46.900	46.360	46.610	47.250	47.340	47.410	47.410	47.110	47.150	47.290	47.000	47.340	47.340	46.780	47.390	46.750	47.280
CaO	0.804	0.860	0.684	0.347	0.321	0.243	0.230	0.440	0.462	0.317	0.574	0.396	0.369	0.325	0.363	0.346	0.256
Na_2O	0.004	0.002	0.015	0.000	0.000	0.004	0.009	0.000	0.000	0.000	0.000	0.004	0.000	0.000	0.000	0.000	0.000
K_2O	0.000	0.006	0.002	0.000	0.004	0.004	0.006	0.000	0.001	0.000	0.000	0.000	0.000	0.000	0.000	0.002	0.000
NiO	0.019	0.015	0.000	0.000	0.015	0.031	0.013	0.010	0.006	0.010	0.010	0.018	0.019	0.025	0.000	0.009	0.010
Total	49.85	49.43	49.39	49.53	49.70	49.52	49.48	49.59	49.68	49.52	49.71	49.78	49.70	48.97	49.58	49.03	49.40

Table 5: Major and trace elements (XRF) of Um Esh serpentinites, Eastern Desert, Egypt.

	Massive serpentinite						**Foliated serpentinite**	
Sample	UE1	UE2	UE3	UE4	UE5	UE6	UE7	UE8
SiO_2	40.441	40.504	37.145	37.477	35.310	33.250	36.739	38.194
TiO_2	0.005	0.004	0.006	0.007	0.009	0.007	0.004	0.004
Al_2O_3	0.600	0.609	0.390	0.385	0.459	0.369	0.568	0.596
Fe_2O_3	7.375	7.403	6.986	6.897	6.630	7.627	7.554	6.930
FeO	0.000	0.000	0.000	0.000	0.000	0.000	0.000	0.000
MnO	0.062	0.059	0.086	0.083	0.124	0.142	0.098	0.089
MgO	38.835	38.842	39.244	39.223	37.629	37.057	38.574	38.759
CaO	0.000	0.000	0.000	0.000	2.834	3.324	0.332	0.112
Na_2O	0.001	0.004	0.008	0.000	0.026	0.020	0.011	0.004
K_2O	0.013	0.012	0.013	0.014	0.018	0.015	0.012	0.016
P_2O_5	0.004	0.004	0.003	0.003	0.004	0.003	0.003	0.003
Cr_2O_3	0.349	0.323	0.320	0.330	0.335	0.254	0.463	0.616
NiO	0.280	0.281	0.330	0.321	0.239	0.212	0.258	0.282
LOI	12.112	12.041	15.531	15.255	16.395	17.730	15.497	14.509
Total	100.08	100.09	100.06	100.00	100.01	100.01	100.11	100.11
Al_2O_3/SiO_2	0.015	0.015	0.011	0.010	0.013	0.011	0.015	0.016
MgO/SiO_2	0.960	0.959	1.056	1.047	1.066	1.115	1.050	1.015
Ba	11.30	10.90	0.00	4.90	2.70	0.00	6.50	19.80
Sr	2.80	0.00	0.00	0.00	48.00	59.10	6.10	2.10
Zr	2.40	7.50	6.70	7.80	7.30	7.20	6.50	7.60
Hf	1.30	1.70	0.90	1.10	1.80	1.90	1.40	0.80
Y	0.00	4.50	3.80	3.90	2.80	3.60	3.70	3.90
Zn	34.90	28.90	41.10	44.80	62.70	43.80	54.00	72.70
Cu	8.80	6.30	6.30	11.00	9.00	13.20	7.50	6.00
Ni	2506	2510	3072	2981	2243	2021	2398	2588
Co	105.5	104.1	128.0	128.0	89.2	92.5	109.4	111.2
Cr	2717	2516	2591	2666	2744	2109	3751	4927
V	26.3	25.0	26.7	25.4	30.3	22.2	32.6	33.7
Sc	6.40	5.90	6.20	8.70	9.30	4.30	3.60	7.40
Th	2.10	0.00	1.40	0.00	0.00	0.00	0.00	0.10
U	0.00	3.30	3.60	5.30	5.40	6.10	4.50	4.20

DISCUSSION

Tectonic setting

The tectonic setting of the ophiolites of the Eastern Desert of Egypt has been controversial. Both subduction-related (e.g. Azer and Stern, 2007; Abd El-Rahman et al., 2009; Basta et al., 2011; Abdel-Karim et al., 2016; Khedr and Arai, 2017) and subduction-unrelated (e.g. Zimmer et al., 1995; Khalil, 2007) settings have been proposed for the Neoproterozoic ophiolites of Egypt. The Al_2O_3/SiO_2 (0.010-0.016) and MgO/SiO_2 (0.96-1.11) values of the Um Esh serpentinites are comparable to those of fore-arc peridotites (Fig. 7), where the fore-arc peridotites are characterized by low Al_2O_3/SiO_2 values. In the extensively serpentinized peridotites, the composition of fresh Cr-spinel has been used as an important petrogenetic indicator (e.g. Barnes and Roeder, 2001). Kamenetsky et al. (2001) suggested that the TiO_2 contents of Cr-spinels can be used to discriminate between peridotites from superasubduction zones (SSZ) and mid-oceanic ridges (MOR). The Al_2O_3 and TiO_2 abundances of the analyzed fresh Cr-spinels overlap those of Cr-spinels of SSZ and MOR peridotites (Fig. 8A). According to Dick and Bullen (1984), the Cr# of fresh Cr-spinel (0.55-0.66) is spanning the range of MOR (Cr# < 0.60) and SSZ (Cr# > 0.60) ophiolites. However, the Mg# (0.39-0.59) and Cr# of the primary Cr-spinel are similar to those of modern SSZ fore-arc peridotites (Fig. 8B). Thus, the protoliths of Um Esh serpentinites are akin to SSZ rather than MOR peridotites.

Nature of Neoproterozoic SSZ Mantle

The low Al_2O_3/SiO_2 (0.010-0.016) values of the Um Esh serpentinites suggest that they represent residual mantle which has experienced high degree of partial melting. The fresh Cr-spinel of Um Esh serpentinite is characterized by very low TiO_2 contents (<0.025 wt%), confirming the depleted nature of these mantle rocks (Jan and Windley, 1990). The primary spinel of harzburgite has Cr# (~0.50) lower than that (~0.70) of Cr-spinel of dunite (Arai and Yurimoto, 1994). Moreover, the Cr# of spinel is proportionally related to the degree of mantle partial melting (Dick and Bullen, 1984). The normative proportions of olivine, orthopyroxene and clinopyroxene of the analyzed samples suggest that the Um Esh serpentinites were formed after harzburgite protolith (Fig. 6). Thus, the higher Cr# (0.55-0.66) of the Um Esh serpentinized harzburgite compared with that of spinel of harzburgite (~0.50, Arai and Yurimoto, 1994) reflects higher degree of partial melting of residual mantle or highly depleted mantle. Moreover, the primary Cr-spinels plot mostly in the field of highly depleted mantle peridotites on the TiO_2 versus Cr# diagram (Fig. 9). In short, the geochemical characteristics of Um Esh serpentinites and their accessory Cr-spinels are consistent with depleted to highly depleted nature of harzburgite mantle.

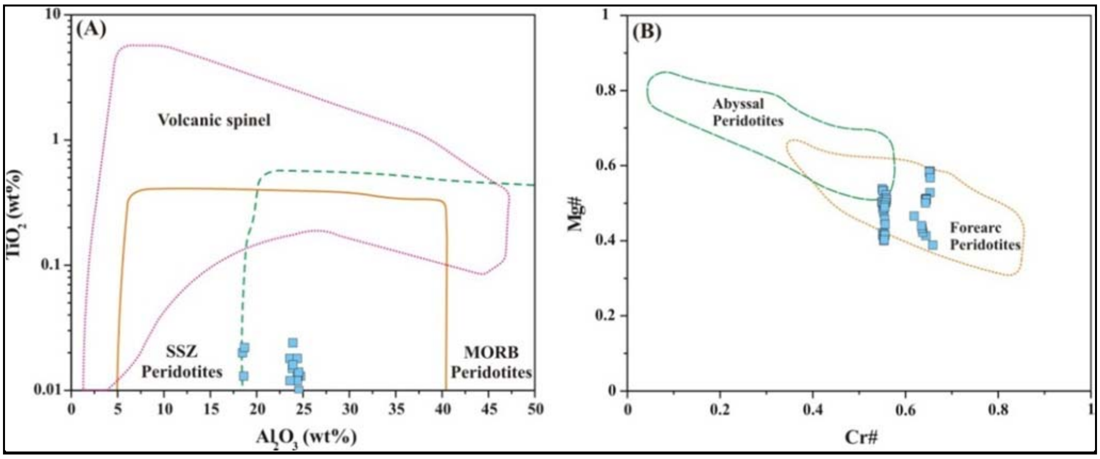

Fig. 8: Tectonic setting of the Um Esh serpentinites. (A) TiO_2 versus Al_2O_3 discrimination diagram (after Kamenetsky et al., 2001), (B) Mg# versus Cr# of the primary Cr-spinel (after Metcalf and Shervais, 2008).

Fig. 9. TiO_2 versus Cr# diagram of the primary Cr-spinel of Um Esh serpentinites (fields after Dick and Bullen, 1984, Jan and Windley, 1990, Arai, 1992).

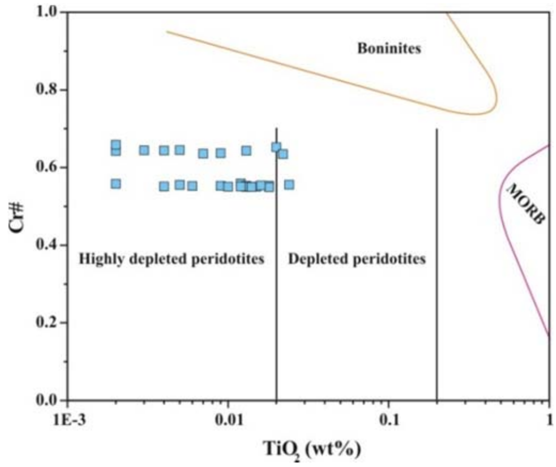

Metamorphism

During low temperature (<300 ^oC) serpentinization of peridotites, olivine and pyroxene are replaced with lizardite/chrysotile. Prograde metamorphism of serpentinites involves transformation of lizardite/chrysotile to antigorite (Derbyshire et al., 2013). Evans et al. (2013) proposed that antigorite grows at the expense of lizardite and chrysotile at temperature above 320 ^oC. The serpentines of Um Esh serpentinite are essentially antigorites (Fig. 5), implying serpentine recrystallization during prograde metamorphism. The Cr-spinel grains of Um Esh serpentinites are usually zoned, with ferritchromite and chromian magnetite (Fig. 2 C and D). The origin of Cr-spinel zonation has been attributed either to serpentinization of ultramafic rocks (e.g. Takla, 1982) or to prograde metamorphism of serpentinized peridotites (e.g. Farahat, 2008; Anzil et al., 2012; Derbyshire et al., 2013). The metamorphic spinel rims are not likely produced during low temperature strongly reducing conditions associated with serpentinization (Derbyshire et al., 2013), which are attributed to production of dihydrogen (H_2) gas as a result of oxidation of ferrous iron in olivine and pyroxene into ferric iron and precipitation of magnetite (Seyfried et al., 2007; Evans, 2010; McCollom et al., 2016; Huang et al., 2017). Moreover, the minimum temperature of formation of ferritchromite is ~500 ^oC (Kimball, 1990; Mellini et al., 2005). Profiles along zoned Cr-spinel grains revealed an increase of Fe^{3+} from fresh spinel through ferritchromite to chromian magnetite (Fig. 4D), suggesting oxidizing conditions during the formation of metamorphic spinel (ferritchromite and chromian magnetite). Plotting the Cr-spinel analyses on the Cr-Al-Fe^{3+} diagram revealed that the ferritchromites were formed at lower amphibolite facies (Fig. 10). Thus, the ferritchromite rims of Cr-spinel of Um Esh serpentinites were produced under oxidizing conditions during prograde (lower amphibolite facies) metamorphism of serpentinites, implying temperature of metamorphism between 500-600 ^oC (Khalil, 2007; Farahat, 2008; González-Jiménez et al., 2009; Abu El-Ela and Farahat, 2011).

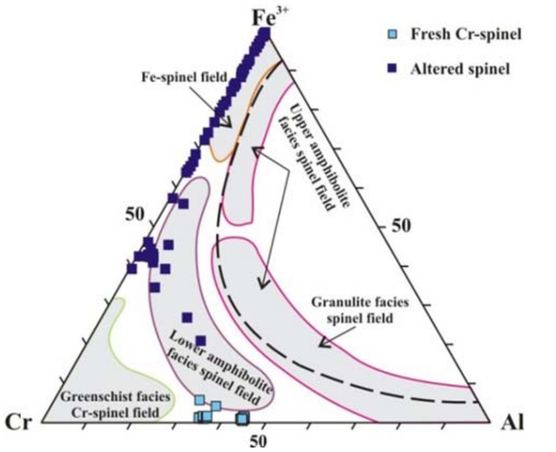

Fig. 10: The composition of primary Cr-spinels and their alteration products plotted on Cr-Al-Fe^{3+} ternary diagram. The fields of different metamorphic facies for Cr-spinel phases and solvus curve (dashed line) are reproduced from Purvis et al. (1972), Evans and Frost (1975), Suita and Strieder (1996) and Barnes and Roeder (2001).

Element mobility during Cr-spinel alteration and metamorphism

Alteration and metamorphism of Cr-spinel result in development of zoned grains (Evans and Frost, 1975) and are accompanied with variation of the abundances of the different elements in the different produced zones (e.g. Khudeir et al., 1992; Azer and Stern, 2007; Khalil, 2007; Farahat, 2008; Abu El-Ela and Farahat, 2011; Derbyshire et al., 2013). Composition profiles along the different zones of the accessory Cr-spinels of Um Esh serpentinites revealed that Al, Mg, Cr and Fe have been exchanged with the surrounding silicates, where Al, Mg and Cr were removed while Fe was added to Cr-spinel (Fig. 4A-C). The higher MnO content of the ferritchromite zones relative to the fresh cores is probably due to addition of Mn released from olivine alteration, whereas the depletion of chromian magnetite rims in MnO relative to ferritchromite (Fig. 4E) can be attributed to accommodation of Mn in the structure of magnesite during progressive metamorphism. This interpretation is supported by the fact that magnesites of Um Esh serpentinites contain up to 0.66 wt% MnO. Similarly, the higher NiO content of the ferritchromite zones and the inner rims of the chromian magnetite zones (Fig. 4F), can be interpreted by addition of Ni from altered olivine, while the depletion of NiO in the outer rims of the chromian magnetite zones can be attributed to donation of Ni to the surrounding serpentines which contain up to 0.91 wt% NiO. The depletion of Ni in only the outer rims of the chromian magnetite zones, compared with MnO depletion in the whole chromian magnetite zone, implies slower diffusion rate of Ni from spinel to the surrounding minerals during metamorphism.

CONCLUSIONS

1- The low Al_2O_3/SiO_2 (0.010-0.016) values of serpentinite samples and the very low TiO_2 contents (<0.025 wt%) of primary Cr-spinels together with Cr# ranging from 0.55 to 0.66 indicate that the Um Esh ophiolite serpentinites represent Neoproterozoic residual harzburgite mantle which experienced high degree of partial melting.

2- The depleted to highly depleted nature of Um Esh serpentinites as reflected by whole-rock geochemical characteristics and mineral chemistry of primary Cr-spinels suggest that these serpentinites are similar to modern SSZ fore-arc peridotites rather than MOR peridotites.

3- The dominance of antigorite and the presence of metamorphic spinel rims suggest that Um Esh serpentinites have experienced prograde metamorphism up to lower amphibolite facies under oxidizing conditions.

4- Composition profiles along the different zones of the accessory Cr-spinels of Um Esh serpentinites revealed that Al, Mg, Cr and Fe have been exchanged with the surrounding silicates, where Al, Mg and Cr were removed while Fe was added to Cr-spinel. Mn and Ni from altered olivine have been added to the Cr-spinel then donated from the chromian magnetite zones to the surrounding magnesite and serpentines, respectively. The diffusion rate of Ni from the chromian magnetite rims to the surrounding silicates was slower than that of Mn.

ACKNOWLEDGEMENTS

Prof. Dr. Chris Heinrich, ETH-Zurich, Switzerland and Prof. Dr. Bottros R. Bakhit, Beni-Suef University, are deeply acknowledged for the laboratory facilities and geochemical analyses without which the present work was not possible.

REFERENCES

Abdel Khalek, M. I., Abdel Maksoud, M. A., Abdel Tawab, M. A. and El-Bedawi, M.A. (1994): An ophiolite-mélange complex south of Dahab, Sinai, Egypt. Ann. Geol. Surv. Egypt, 20, 1-18.

Abd El-Rahman, Y., Ploat, A., Dilek, Y., Fryer, B., El-Sharkawy, M. and Sakran, S. (2009): Geochemistry and tectonic evolution of the Neoproterozoic Wadi Ghadir Ophiolite, Eastern Desert, Egypt. Lithos, 113 (1-2), 158-178.

Abdel-Karim, A. M., Ali, S., Helmy, H. M. and El-Shafei, S. A. (2016): Fore-arc setting of the Gerf ophiolite, Eastern Desert, Egypt: evidence from mineral chemistry and geochemistry of ultramafites. Lithos, 263, 52-65.

Abu El-Ela, F. F. and Farahat, E. S. (2011): Neoproterozoic podiform chromitites in serpentinites of the Abu Meriewa-Hagar Dungash district, Eastern Desert, Egypt: geotectonic implications and metamorphism. Island Arc, 19, 151-164.

Abu El-Enen M. M. and Makroum F. M. (2003): Tectonometamorphic evolution of the northeastern Kid Belt, Southeast Sinai, Egypt. Ann. Geol. Surv. Egypt, 26, 19-37.

Akaad, M.K. and Noweir, A.M. (1980): Geology and lithostratigraphy of the Arabian Desert orogenic belt of Egypt between latitudes 25° 35′ and 26° 30′ N. Inst. App. Geol. Bull., Jeddah, 2, 127-136.

Ahmed, A. H. (2013): Highly depleted harzburgite-dunite-chromitite complexes from the Neoproterozoic ophiolite, south Eastern Desert, Egypt: a possible recycled upper mantle lithosphere. Precamb. Res., 233, 173-192.

Ahmed, A. H., Arai, S. and Attia, A.K. (2001): Petrological characteristics of podiform chromitites and associated peridotites of the Pan African ophiolite complexes of Egypt. Mineral. Deposita, 36, 72-84.

Ahmed, A. H., Harbi, H. M. and Habtoor, A. M. (2012): Compositional variations and tectonic settings of podiform chromitites and associated ultramafic rocks of the Neoproterozoic ophiolite at Wadi Al Hwanet, northwestern Saudi Arabia. J. Asian Earth Sci., 56, 118-134.

Ali, K. A., Azer, M.K., Gahlan, H. A., Wilde, S. A., Samuel, M.D. and Stern, R.J. (2010): Age constraints on the formation and emplacement of Neoproterozoic ophiolites along the Allaqi-Heiani suture, South Eastern Desert of Egypt. Gond. Res., 18, 583-595.

Andresen, A., El-Rus, M. A. A., Myhre, P. I. and Boghdady, G. Y. (2009): U-Pb TIMS age constraints on the evolution of the Neoproterozoic Meatiq Gneiss Dome, Eastern Desert, Egypt. Inter. J. Earth Sci., 98, 481-497.

Anzil, P. A., Guereschi, A. B. and Martino, R. D. (2012): Mineral chemistry and geothermometry using relict primary minerals in the La Cocha ultramafic body: a slice of the upper mantle in the Sierra Chica of Cordoba, Sierras Pampeanas, Argentina. J. South Amer. Earth Sci., 40, 38-52.

Arai, S. (1992): Chemistry of chromian spinel in volcanic rocks as a potential guide to magma chemistry. Mineral. Mag., 56, 173-184.

Arai, S. and Yurimoto, H. (1994): Podiform chromitites of Tari-misaka ultramafic complex, southwest Japan, as mantle-melt interaction products. Econ. Geol., 89, 1279-1288.

Azer, M. K. and Stern, R. J. (2007): Neoproterozoic (835-720 Ma) serpentinites in the Eastern Desert, Egypt: fragments of forearc mantle. J. Geol., 115, 457-472.

Bakhit, B.R. (1994): Gold mineralization in some occurrences of the Eastern Desert, Egypt. M. Sc Thesis, Cairo Univ., 214p.

Bakhit, B. R. (2002): Geology, mineralogy and genesis of some gold occurrences, Eastern Desert, Egypt. Ph. D Thesis, Cairo Univ., 300p.

Barnes, S. J. and Roeder, P. L. (2001): The range of spinel compositions in terrestrial mafic and ultramafic rocks. J. Petrol., 42, 2279-2302.

Basta, F.F. (1983): Geology and geochemistry of the ophiolitic mélange and other rock units in the area around and west of Gabal Ghadir, Eastern Desert, Egypt. Ph.D. thesis, Cairo Univ., 137p.

Basta, F. F., Maurice, A. E., Bakhit, B. R., Ali, K. A. and Manton, W. I. (2011): Neoproterozoic Contaminated MORB of Wadi Ghadir Ophiolite, NE Africa: Geochemical and Nd and Sr isotopic Constraints. J. Afr. Earth Sci., 59, 227-242.

Basta, F. F., Maurice, A. E., Bakhit, B. R., Azer, M. K. and El-Sobky, A. F. (2017): Intrusive rocks of the Wadi Hamad area, North Eastern Desert, Egypt: change of magma composition with maturity of Neoproterozoic continental island arc and the role of collisional plutonism in the differentiation of arc crust. Lithos, 288-289, 248-263.

Coleman, R. G. (1977): Ophiolites. Springer-Verlag, Berlin, 229 p.

Derbyshire, E. J., O'Driscoll, B., Lenaz, D., Gertisser, R. and Kronz, A. (2013): Compositionally heterogeneous podiform chromitite in the Shetland Ophiolite Complex (Scotland): Implications for chromitite petrogenesis and late-stage alteration in the upper mantle portion of a supra-subduction zone ophiolite. Lithos, 162-163, 279-300.

Dick, H. B. and Bullen, T. (1984): Chromian spinel as a petrogenetic indicator in abyssal and Alpine-type peridotites and spatially associated lavas. Contrib. Mineral. Petrol., 86, 54-76.

Dilek, Y. and Furnes, H. (2011): Ophiolite genesis and global tectonics: Geochemical and tectonic fingerprinting of ancient oceanic lithosphere. Geol. Soc. Amer. Bull., 123, 387-411.

Dilek, Y. and Furnes, H. (2014): Ophiolites and their origins. Elements 10, 93-100.

Dungan, M. A. (1979): A microprobe study of antigorite and some serpentine pseudomorphs. Amer. Mineral., 17, 771-784.

El-Amawy, M. A., Wetait, M. A., Mehanna, A. M., Soliman, F. A. and Ghabour, Y. (2004): Geology and structural evolution of the basement rocks of Imlig area, southwest Sinai, Egypt. Ann. Geol. Surv. Egypt, 27, 19-33.

El-Sayed, M. M., Furnes, H. and Mohamed, F. H. (1999): Geochemical constraints on the tectonomagmatic evolution of the late Precambrian Fawakhir ophiolite, Central Eastern Desert, Egypt. J. Afr. Earth Sci., 29 (3), 515-533.

El-Sharkawy, M. A. and El-Bayoumi, R. (1979): The ophiolites of Wadi Ghadir area, Eastern Desert, Egypt. Ann. Geol. Surv. Egypt, 9, 125-135.

Evans, B. W. (2010): Lizardite versus antigorite serpentinite: magnetite, hydrogen and life (?). Geology, 38, 879-882.

Evans, B. W. and Frost, B. R. (1975): Chrome-spinel in progressive metamorphism - a preliminary analysis. Geochim. Cosmochim. Acta, 39, 959-972.

Evans, B. W., Hattori, K. and Baronnet, A. (2013): Serpentinite: what, why, where?. Elements, 9, 99-106.

Farahat, E. S. (2008): Chrome-spinels in serpentinites and talc carbonates of the El Ideid-El-Sodmein District, central Eastern Desert, Egypt: their metamorphism and petrogenetic implications. Chem. Erde, 68, 193-205.

Franz, L. and Wirth, R. (2000): Spinel inclusions in olivine of peridotite xenoliths from TUBAF seamount (Bismarck Archipelago/Papua New Guinea): evidence for the thermal and tectonic evolution of the oceanic lithosphere. Contrib. Mineral. Petrol., 140, 283-295.

Gahlan, H. A., Arai, S., Abu El-Ela, F. F. and Tamura, A. (2012): Origin of wehrlite cumulates in the Moho transition zone of the Neoproterozoic Ras Salatit ophiolite, Central Eastern Desert, Egypt: crustal wehrlites with typical mantle characteristics. Contrib. Mineral. Petrol., 163, 25-241.

González-Jiménez, J. M., Kerestedjian, T., Proenza, J. A. and Gervilla, F., (2009): Metamorphism on chromite ores from the Dobromirtsi Ultramafic Massif, Rhodope Mountains (SE Bulgaria). Geol. Acta, 7, 413-429.

Harraz, H. (1995): Primary geochemical haloes, El Sid gold mine, Eastern Desert, Egypt. J. Afr. Earth Sci. 20, 61-71.

Hart, S. R. and Zindler, A. (1986): In search of a bulk-earth composition. Chem. Geol., 57, 247-267.

Huang, R., Lin, C.-T., Sun, W., Ding, X., Zhan, W. and Zhu, J. (2017): The production of iron oxide during peridotite serpentinization: influence of pyroxene. Geosci. Front., 8, 1311-1321.

Jan, M. Q. and Windley, B.F. (1990): Chromian spinel-silicate chemistry in ultramafic rocks of the Jijal complex, northwestern Pakistan. J. Petrol., 31, 667-715.

Jagoutz, E., Palme, H., Baddenhausen, H., Blum, K., Cendales, M., Dreibus, G., Spettel, B., Lorenz, V. and Vanke, H. (1979): The abundance of major, minor and trace elements in the earth's mantle as derived from primitive ultramafic nodules. Geochim. Cosmochim. Acta, 11 (2), 2031-2050.

Khedr, M. Z. and Arai, S. (2017): Peridotite-chromitite complexes in the Eastern Desert of Egypt: Insight into Neoproterozoic sub-arc mantle processes. Gond. Res., 52, 59-79.

Kamenetsky, V., Crawford, A.J. and Meffre, S. (2001): Factors controlling chemistry of magmatic spinel: an empirical study of associated olivine, Cr-spinel and melt inclusions from primitive rocks. J. Petrol., 42, 655-671.

Khalil, K. I. (2007): Chromite mineralization in ultramafic rocks of the Wadi Ghadir area, Eastern Desert, Egypt: mineralogical, microchemical and genetic studies. N. Jb. Miner. Abh., 183, 283-296.

Kimball, K. (1990): Effects of hydrothermal alteration on the composition of chromian spinels. Contrib. Mineral. Petrol., 105, 337-346.

Kröner, A., Todt, W., Hussein, I. M., Mansour, M. and Rashwan, A. A. (1992): Dating of late Proterozoic ophiolites in Egypt and the Sudan using the single grain zircon evaporation technique. Precamb. Res., 59, 15-32.

Khudeir, A. A., El-Haddad, M. A. and Leake, B. E. (1992): Compositional variation in chromite from the Eastern Desert, Egypt. Mineral. Mag., 56, 567-574.

Madbouly, M. I. (2000): A comparative study on petrology and geochemistry of some mafic-ultramafic intrusions of the Eastern Desert and Sinai, Egypt. Ph. D. Thesis, Cairo Univ., 262 p.

McCollom, T.M., Klein, F., Robbins, M., Moskowitz, B., Berquó, T.S., Jöns, N., Bach, W. and Templeton, A. (2016): Temperature trends for reaction rates, hydrogen generation, and partitioning of iron during experimental serpentinization of olivine. Geochim. Cosmochim. Acta, 181, 175-200.

Mehanna, A.M., Wetait, M.A., El-Amawy, M.A., Solimani, F.A. and Ghabour, Y. (2004): Petrogenesis and metamorphism of the basement rocks of Imlig area, southwest Sinai, Egypt. Ann. Geol. Surv. Egypt, 27, 35-59.

Mellini, M., Rumori, C. and Viti, C. (2005): Hydrothermally reset magmatic spinels in retrograde serpentinites: formation of ‘ferritchromit’ rims and chlorite aureoles. Contrib. Mineral. Petrol., 149, 266-275.

Metcalf, R. V. and Shervais, J. W. (2008): Suprasubduction-zone ophiolites: is there really an ophiolite conundrum? Geol. Soc. Amer. Special Paper 438, 191-222.

Niu, Y. (2004): Bulk-rock major and trace element compositions of abyssal peridotites: implications for mantle melting, melt extraction and post-melting processes beneath mid-ocean ridges. J. Petrol., 45, 2423-2458.

Parkinson, I. J. and Pearce, J. A. (1998): Peridotites of the Izu-Bonin-Mariana forearc (ODP Leg 125) evidence for mantle melting and melt-mantle interactions in a supra-subduction zone setting. J. Petrol., 39, 1577-1618.

Pearce, J. A. (2014): Immobile element fingerprinting of ophiolites. Elements, 10, 101-108.

Pearce, J. A., Barker, P. F., Edwards, S. J., Parkinson, I. J. and Leat, P. T. (2000): Geochemistry and tectonic significance of peridotites from the South Sandwich arc-basin system, South Atlantic. Contrib. Mineral. Petrol., 139, 36–53.

Purvis, A. C., Nesbitt, R. W. and Halberg, J. A. (1972): The geology of part of Carr Boyd Complex and its associated nickel mineralization, Western Australia. Econ. Geol., 67, 1093-1113.

Schwartz, S., Guillot, S., Reynard, B., Lafay, R., Debret, B., Nicollet, C., Lanari, P. and Auzende, A. L. (2013): Pressure-temperature estimates of the lizardite/antigorite transition in high pressure serpentinites. Lithos, 178, 197-210.

Seyfried Jr., W. E., Foustoukos, D.I. and Fu, Q. (2007): Redox evolution and mass transfer during serpentinization: an experimental and theoretical study at 200 ^{o}C, 500 bar with implications for ultramafic-hosted hydrothermal systems at mid-ocean ridges. Geochim. Cosmochim. Acta, 71, 3872-3886.

Shimron, A. E. (1981): The Dabab mafic-ultramafic complex. A probable ophiolite of late Proterozoic (Pan-African) age. Ofioliti, 6, 161-164 .

Shimron, A.E. (1984): Evolution of the Kid Group, southeast Sinai Peninsula: thrusts, mélanges, and implications for accretionary tectonics during the Proterozoic of the Arabian–Nubian Shield. Geology, 12, 242-247.

Suita, M. T. and Strieder, A. J. (1996): Cr-spinels from Brazilian mafic-ultramafic complexes: metamorphic modifications. Inter. Geol. Rev., 38, 245-267.

Stern, R. J. (1994): Arc assembly and continental collision in the Neoproterozoic East-African Orogen - implications for the consolidation of Gondwanaland. Ann. Rev. Earth Planet. Sci., 22, 319-351.

Takla, M. A. (1982): Chromites from the Bergen arcs ultramafics, southern Norway. N. Jb. Miner. Abh., 144, 56-72.

Takla, M. A., Basta, F. F., Madbouly, M. I. and Hussein, A. A. (2001): The mafic-ultramafic intrusions of Sinai, Egypt. Ann. Geol. Surv. Egypt, 24, 1-40.

Taman, Z. (1996): Geology and mineralization of Wadi Atalla area, Eastern Desert, Egypt. MSc thesis, Ain Shams Univ., 120 p.

Wassef, B., Kamel, O. A., Armanious, L. K. and Sabet, A. H. (1973): Report on the results of the prospecting work for gold in El Sid-Semna area in 1970/1971. Geol. Surv. Egypt, internal report no. 23/1973.

Zimmer, M., Kröner, A., Jochum, K. P., Reischmann, T. and Todt, W. (1995): The Gabal Gerf complex: A Precambrian N-MORB ophiolite in the Nubian Shield, NE Africa. Chem. Geol., 123, 29-51.

Zoheir, B., Deshesh, F., Broman, C., Pitcairn, I., El-Metwally, A. and Mashaal, S. (2018): Granitoid-associated gold mineralization in Egypt: A case study from the Atalla mine. Mineral. Deposita, 53, 701-720.

بترولوجية وجيوكيميائية سربنتين أوفيوليتى بمنطقة أم عش، الصحراء الشرقية، مصر: وشاح نيوبروتيروزوى من بيئة فوق نطاق الإندساس متحول

أيمن البدرى موريس

قسم الجيولوجيا – كلية العلوم – جامعة حلوان

الخلاصة

يشتمل السربنتين الأوفيوليتى النيوبروتيروزوى لمنطقة أم عش بوسط الصحراء الشرقية المصرية على أنواع كتلية ومرققه والتى تتكون أساساً من معدن الأنتيجوريت مع قليل من معدن الكروم سبينيل. تتمثل معادن الكربونات بالماجنيزيت الذى يتواجد فى شكل تجمعات أو عُريقات. تكون حبيبات الكروم سبينيل متنطقه دائماً، من لُب طازج أو بقايا طازجه محاطة بحواف من الفريت كروميت والماجنيتيت الحاوى على الكروم. يتميز الكروم سبينيل الأوّلى بمحتوى قليل جداً من أكسيد التيتانيوم (أقل من ٠.٠٢٥ %) وكذلك قيم قليلة (٠.٠١٠ –٠.٠١٦) لنسبة أكسيد الألومنيوم إلى أكسيد السيليكون مما يوضح أن صخور السربنتين تمثل وشاح متبقى تعرّض لدرجه عالية من الأنصهار الجزئى. ويتشابه محتوى الكروم سبينيل الأوّلى من أكسيد الألومنيوم (١٦–٢٥%) وأكسيد التيتانيوم (٠.٠٠٧ % فى المتوسط) مع تلك التى لصخور البريدوتيت المتكونه فى بيئة فوق نطاق الإندساس وبيئة تلال وسط المحيط. ولكن الطبيعة شديدة الإستنضاب لسربنتين منطقة أم عش وكذلك ال Cr# و Mg# للكروم سبينيل الأوّلى تتشابه مع تلك التى لصخور البريدوتيت المتكون أمام القوس لبيئة فوق نطاق الإندساس.

وأظهرت قطاعات للتركيب الكيميائى للنطاقات المختلفة للكروم سبينيل المتنطق أن تركيزات أكاسيد الكروم والمغنسيوم والألومنيوم قد إنخفضت فجأة بينما إزدادت بسرعة تركيزات أكسيد الحديد وكذلك Fe# من الكروم سبينيل الطازج إلى الفريت كروميت إلى الماجنيتيت الحاوى على الكروم، كما أن التغير فى تركيزات تلك الأكاسيد كان متدرجاً داخل النطاق الواحد من نطاقات السبينيل المتحول. وعلى الجانب الأخر فأن تركيزات أكاسيد النيكل والمنجنيز تتغير بشكل غير منتظم من اللُب إلى الحافة .

تؤكد سيادة معدن الأنتيجوريت فى صخور السربنتين ووجود حواف من السبينيل المتحول حول الكروم سبينيل الأوّلى أن صخور سربنتين أم عش قد تعرضت إلى تحول فى سحنة الأمفيبوليت السفلى فى ظروف بيئة مؤكسدة.